

# HIGH TEMPERATURE DIELECTRIC PROPERTIES OF GOETHITE FROM 400 to 3000 MHz

C. A. Pickles  
Department of Mining Engineering  
Queen's University  
Kingston, Ontario  
Canada, K7L-3N6

AND

J. Mouris and R. M. Hutcheon  
Microwave Properties North (MPN)  
Deep River, Ontario  
Canada, K0J-1P0

## ABSTRACT

The dielectric properties of goethite and, in particular, the changes during the topotactic conversion of goethite to hematite, were studied from room temperature to about 800°C in the frequency range of 400 to 3000 MHz using the cavity perturbation technique. The complex permittivity, i.e. both the real and the imaginary or absorptive parts ( $\epsilon'$  and  $\epsilon''$ ) were measured under various heating regimens. In addition, Thermogravimetric Analysis (TGA) was performed in order to characterize the transformation of goethite to hematite. The Debye relaxation formalism was applied to the processes occurring both during and after the main dehydroxylation reaction in order to calculate the relaxation times. The Arrhenius equation for thermally activated relaxation times was used to determine the activation energies.

Both the real and the absorptive parts of the permittivity exhibited a significant peak during the main part of the goethite to hematite decomposition reaction. Above the transformation, there was another, less dramatic, thermally activated increase in the

permittivity values. The increase in the permittivities during the goethite to hematite transformation was attributed to the formation of quasi-free migrating radicals, e.g. hydroxyl ions, oxygen ions or hydrogen atoms, during the dehydroxylation of goethite. The Derivative Thermogravimetric Analysis (DTGA) curve was found to be directly related to the transient values of the real and the imaginary permittivities. Higher heating rates resulted in an accelerated rate of dehydroxylation and therefore higher values of the transient permittivities. In the temperature range of 400°C to 500°C, i.e. just above the dehydroxylation peak, the real permittivity exhibited a varying frequency dependence, which suggested that changes were occurring in the newly formed, highly defected hematite structure, which is referred to as hydrohematite. During the reaction there were multiple relaxation processes and thus the Debye relationship could not be applied. However, at temperatures above about 500°C, the structure stabilized, the Debye relationship was more closely followed, and the relaxation times could be determined as a function of temperature. The activation energy for the relaxation process above 500°C was determined to be 0.47 kJ/mole.

## INTRODUCTION

Goethite is a major mineralogical component of a number of ores, in particular bauxite, which is the raw material for activated alumina production (1, 2) and for the manufacture of aluminum metal (1, 2). The thermal decomposition of goethite ( $\alpha$ -FeOOH) to hematite ( $\alpha$ -Fe<sub>2</sub>O<sub>3</sub>) is a reaction of considerable industrial importance, since there are a number of applications for  $\alpha$ -Fe<sub>2</sub>O<sub>3</sub>, such as in pigment manufacture (3), magnetic recording oxides (4) and ferrites (5). The overall reaction can be described by the following equation:



The present research was undertaken in order to improve the understanding of the microwave heating and dissociation characteristics of goethite as a function of temperature and frequency. Firstly, the literature regarding the thermal transformation of goethite to hematite has been reviewed, followed by a discussion of the fundamental parameters which govern microwave processing, e.g. the real and the imaginary permittivities and the loss tangent. The real and the imaginary parts of the complex scalar permittivities of the mineral goethite were measured using the cavity perturbation technique at six frequencies in the range of 397 MHz to 2986 MHz, up to temperatures of about 800°C. Also, since the thermal dehydroxylation of goethite results in a phase change with a significant mass loss, then Thermogravimetric Analysis (TGA) was performed in order to characterize the transformation reaction. From the TGA results, the Derivative Thermogravimetric Analysis (DTGA) curves were calculated and related to the permittivities.

#### *Goethite to Hematite Transformation*

It has been proposed that the thermal dehydration of goethite leads to complete conversion into a “hematite-like” phase before less than one-half of the water has been removed from the goethite (6-9). First, an intermediate species is produced with the general chemical formula:  $\alpha\text{-Fe}_{2-x/3}(\text{OH})_x\text{O}_{3-x}$  where the x-value is approximately equal to 1.0. This chemically and structurally distinct species is often referred to as protohematite in the literature (10). Furthermore, it has been suggested that as dehydration proceeds, the hydroxyl groups ( $\text{OH}^-$ ) replace the oxygen ions ( $\text{O}^{2-}$ ) in the hematite structure and the

hydroxyl radicals form associations with vacancies in the cation sub-lattice (6). Before complete conversion to  $\alpha\text{-Fe}_2\text{O}_3$  is achieved, a second distinguishable intermediate phase, termed hydrohematite (11), is produced with an x-value of 0.5 at temperatures in the range of 400°C to 600°C.

On the other hand, other authors have argued that these intermediate phases do not exist and have developed physical models to describe the transformation (12, 13). With conventional heating processes, thermal dehydration advances from the surface to the interior of the goethite and a compact surface layer of hematite forms. This layer acts as a barrier, which hinders the further dehydroxylation of the remaining goethite and thus the reaction enthalpy increases with increasing particle size. Additional support for this model was provided by a second peak in the Differential Thermal Analysis (DTA) curves of the goethite samples (13).

Differences in the behaviours of various goethite samples can be attributed to the different chemical and physical properties of the goethites. It has been shown previously that the dehydroxylation of goethite can be affected by particle size and structural defects (14), aluminum substitution (15) and excess or non-stoichiometric hydroxyl ions (16, 17). Decreasing particle size and increasing numbers of structural defects promote dehydroxylation. Aluminum substitution raises the dehydroxylation temperature, since diaspore ( $\text{AlOOH}$ ) is more stable than goethite. The presence of excess or non-stoichiometric hydroxyl ions can reduce the transformation temperature. Goethite, which is synthesized from ferrous ions ( $\text{Fe}^{2+}$ ) can have a lower dehydroxylation temperature

than goethite produced from ferric ions ( $\text{Fe}^{3+}$ ) since the goethite from the  $\text{Fe}^{2+}$  ions can have excess hydroxyl units (18).

More recently, Ruan et al utilized Fourier Transform Infrared Spectroscopy (FT-IR) to study the reaction and found that the hydroxyl units were observed in the hydroxyl stretching and hydroxyl deformation and water bending regions (19). The spectrum of goethite showed two significant hydroxyl vibrations in the hydroxyl stretching region, which were characteristic of the stoichiometric and non-stoichiometric hydroxyl units. During the transformation, hydroxyl units were liberated, but the resulting hematite inherited both the stoichiometric and the non-stoichiometric types. Hydroxyl units can remain in the hematite structure even up to  $900^\circ\text{C}$  (20-22).

#### *Dielectric Heating Formalism*

The degree of interaction of microwaves with a material depends on both the dielectric and the magnetic properties of the medium and these can be described in terms of the complex permittivity ( $\epsilon$ ) and the complex permeability ( $\mu$ ), respectively. For a material, which does not have significant magnetic properties, then only the complex permittivity need be considered. The rate of microwave energy absorption by a material at a specific temperature (T) is related to the complex permittivity ( $\epsilon$ ), which is defined at a given temperature (T) as follows:

$$\epsilon(T) = \epsilon_0 [\epsilon'_r(T) - j\epsilon''_r(T)] \quad (2)$$

where  $\epsilon_0$  is the permittivity of free space ( $8.86\text{E-}12$  F/m),  $\epsilon'_r$  is the relative real component of the complex permittivity,  $\epsilon''_r$  is the relative imaginary part of the complex

permittivity and  $j = (-1)^{1/2}$ . The relative real part of the complex permittivity, i.e. the relative real permittivity ( $\epsilon'_r$ ), is often referred to as the relative dielectric constant and is a measure of the high frequency electrical polarizability of the material. In most cases, it is relatively constant at low temperatures but usually increases at high temperatures. The relative permittivity is the ratio of the actual permittivity to that of free space, i.e.  $\epsilon'_r = \epsilon'/\epsilon_0$  and  $\epsilon''_r = \epsilon''/\epsilon_0$ .

According to the Debye relation, the real part of the permittivity ( $\epsilon'$ ) at a given radial frequency ( $\omega$ ) can be defined as follows:

$$\epsilon'(\omega) = \epsilon'_\infty + \frac{\epsilon'_s - \epsilon'_\infty}{1 + \omega^2 \tau^2} \quad (3)$$

where  $\epsilon'_\infty$  is the high frequency limiting value of  $\epsilon'$ ,  $\epsilon'_s$  is the static value of  $\epsilon'$ ,  $\omega = 2\pi f$  is the radial frequency and  $f$  is the frequency of the incident wave in Hz, and  $\tau$  is the time constant or the relaxation time of the polarization process in seconds. This equation is usually applied to liquids but can be applied to solids in cases where a dipole-producing unit is free to move in the material. At low temperatures, the numerical value of the real permittivity is due to charge polarization, i.e. slight displacements of electrons and ions from their normal lattice sites. Since this process is usually very rapid then it is essentially frequency independent. Furthermore, any loss mechanisms involving the movement of electrons or ions will affect the value of the real permittivity, but the magnitude of this effect will depend on the relaxation rate of the mechanism. If the relaxation rate is higher than the microwave frequency then the real permittivity will not be strongly influenced. Standard conduction electron losses, i.e. normal resistivity losses,

usually have very fast relaxation times and produce a larger contribution to the imaginary permittivity than the real permittivity.

The imaginary part of the complex permittivity ( $\epsilon''$ ), or the dielectric loss factor, characterizes the ability of the material to convert electrical energy to random thermal kinetic energy of motion. It will be dependent on the temperature and the microwave frequency. According to the Debye relationship, the imaginary permittivity of a relaxing dipole species can be defined at a given radial frequency ( $\omega$ ) as follows:

$$\epsilon''(\omega) = \frac{(\epsilon'_s - \epsilon'_\infty)\omega\tau}{1 + \omega^2\tau^2} \quad (4)$$

At low temperatures, the real part of the permittivity is usually much larger than the imaginary part. The numerical value of the imaginary permittivity is a result of the movement of defects, i.e. ions into vacancies or ions into interstitial sites or to the movement of electrons in traps. The absolute value of the contribution of these to the imaginary permittivity will depend on both their number and their rate of movement. These phenomena are temperature dependent but are independent of the frequency if the thermally induced hopping rate is significantly higher than the microwave frequency. At low temperatures, this is usually the case for most materials. In contrast to the real permittivity, the imaginary permittivity will be significantly affected by loss mechanisms involving the movement of electrons or ions, even if the relaxation rate of the mechanism is much higher than the frequency. If the predominant loss mechanism is thermally activated ion or electron conduction then the values of the imaginary permittivity ( $\epsilon''$ ) should show an inverse dependency on the frequency

A common indicator of the general magnitude of microwave losses is the loss tangent ( $\tan\delta$ ) as follows:

$$\tan\delta = \frac{\varepsilon''}{\varepsilon'} \quad (5)$$

and substituting equations (3) and (4) into equation (5) gives:

$$\tan\delta = \frac{(\varepsilon'_s - \varepsilon'_\infty)\omega\tau}{\varepsilon_s + \varepsilon_\infty\omega^2\tau^2} \quad (6)$$

The half-power penetration depth (D), which is defined as the depth where the incident power is reduced by one-half, is related to the loss tangent and can be approximated as follows:

$$D = \frac{3\lambda_o}{8.868\pi \tan \delta (\varepsilon')^{1/2}} \quad (7)$$

where  $\lambda_o$  is the incident or free-space wavelength. From this equation it can be seen that the penetration depth is inversely proportional to the frequency of the microwave radiation. Although low frequencies result in greater penetration depths, the actual amount of heating may not be significantly increased if the internal field,  $E_{int}$ , is low. However, again the actual amount of heating is strongly dependent on the properties of the material.

## **EXPERIMENTAL DETAILS**

### *Raw Materials*

The goethite mineral ( $\alpha$ -FeO·(OH)) was obtained from Ward's Natural Science and had the following composition: 92.75 %FeO·(OH), 3.45 %SiO<sub>2</sub>, 0.09 %Al<sub>2</sub>O<sub>3</sub>, 0.19 %CaO, 0.27 %MgO, 0.05 %Na<sub>2</sub>O, 0.04 %K<sub>2</sub>O, 1.84 %MnO, 0.02 %TiO<sub>2</sub>, 0.09%P<sub>2</sub>O<sub>5</sub>, <0.01 %Cr<sub>2</sub>O<sub>3</sub>, 0.85 %H<sub>2</sub>O.

### *Thermogravimetric Analysis*

Thermogravimetric Analysis (TGA) was performed on a Netzsch STA-409 high temperature (1575°C) DTA, which can also provide simultaneous TGA. The samples, weighing a few hundred milligrams, were placed in an alumina crucible and the heating rate was 7.5 °C/min in air. The Derivative Thermogravimetric Analysis (DTGA) data are the slope values as calculated from the TGA results and 1 %/°C is equivalent to 7.5 %/min.

#### *Dielectric Constant Measurements*

The fundamental microwave parameters were measured by the cavity perturbation technique, which is based on measuring the difference in the microwave cavity response between a cavity with an empty sample-holder and a cavity with a sample-holder plus the sample (23, 24). In this technique, the apparent interaction between the microwaves and the sample is increased to induce a measurable attenuation. This is achieved by amplifying the electric field by the quality factor,  $Q$ . If the sample size is small enough, such that the conventional perturbation theory can be applied, then the permittivity of the material varies linearly with the resonant frequency and the  $Q$ -factor shifts. The system can measure the dielectric properties at frequencies between 50 MHz and 3 GHz, up to a temperature of about 1400°C. In most cases, the measurements are usually made at frequencies of 915 MHz and 2460 MHz, which are the internationally agreed and recognized frequency bands.

The sample powders were compressed in a tungsten carbide lined die at about 20,000 psi in a uniaxial press to form briquettes with a diameter of about 3.5 mm and a length of about 4 mm. The briquettes were weighed and their density was determined to be 2.98 gm/cc. The sample (a stack of three pellets weighing 0.455 gm) was placed into a high

purity amorphous silica (low OH content) cylindrical tube (wall thickness 1 mm, outer diameter 6 mm) with an internal shelf to support the sample. The tube was cleaned, dried and heated to 500°C before each test.

A schematic diagram of the major components of the cavity perturbation measurement system is shown in Figure 1. The holder, with the sample in it, was heated in a conventional resistance furnace and then rapidly removed and inserted into the high electric field region of a thick-walled, well-cooled  $TM_{0n0}$  cavity. The  $TM_{0n0}$  resonator is a 580 mm diameter, 50 mm long right cylindrical cavity (fundamental mode at 400 MHz) which, with a 12 mm long, 3.5 mm diameter sample inserted along the axis, has clearly separated modes up to a  $n = 6$  at 2970 MHz. The cavity is a furnace-brazed, thick-walled OFHC copper structure with cooling channels machined into the central axial region, which is exposed to the high temperature sample holder plus sample. The unloaded  $Q$ -factor of this cavity is approximately 10,000 at 400 MHz and increases to over 30,000 for the  $n = 6$  mode. The thermal transient produced by inserting the hot sample produces small shifts in frequency, but the effect of these is minimized by performing the hot empty sample holder measurements with the same time delays and frequency sequences used during the measurements with the sample holder plus the sample.

The resonant frequency and loaded quality factor,  $Q$ , of the cavity were measured by a Hewlett-Packard 8753 network analyzer and stored for off-line analysis, which includes the subtraction of the hot empty sample holder effects. The peak-analysis and frequency-agile abilities of the Hewlett-Packard 8753 network analyzer allows for measurements at half-a-dozen frequencies in less than ten seconds. The sample holder was continuously flushed with high purity argon gas. After the measurement, the sample and holder were

quickly returned to the furnace for further processing. The sample was held at temperature for at least five minutes to ensure that equilibrium was achieved at a given temperature in the resistance furnace. Two heating rates of 3.2°C/min and 7.5°C/min in an air atmosphere were employed. At the completion of the test, the mass of the sample and the sample dimensions were re-measured. The empty sample holder values were obtained using the same technique at 100°C intervals up to the maximum selected temperature. Then, assuming linear behavior, the empty holder measurements were subtracted from the sample plus holder measurements.

The data analysis employs the general formalism of resonant cavity frequency shift theory, in which the real ( $\chi'_e$ ) and the imaginary parts ( $\chi''_e$ ) of the complex electric susceptibility ( $\chi_e = \chi'_e - j\chi''_e$ ) are related, through functions, which are dependent on the sample shape, to the change in cavity resonant frequency and the  $Q$ -factor through the following equation (23, 24):

$$\frac{\Delta f}{f_E} + j \left( \frac{1}{2Q_{LS}} - \frac{1}{2Q_{LE}} \right) = \left( \frac{-\chi_e}{1 + \chi_e F_{sh}} \right) \left( \frac{V_s}{V_c} \right) A \quad (8)$$

where  $f_E$  is the cavity frequency,  $Q_{LE}$  is the loaded cavity  $Q$  with the empty sample holder,  $\Delta f$  is the frequency shift produced by the sample,  $Q_{LS}$  is the loaded cavity  $Q$  with both the holder and the sample,  $F_{sh}$  is a real number which is dependent on only the sample shape,  $V_s$  and  $V_c$  are the respective sample and cavity volumes, and  $A$  is a real calibration constant which is dependent on only the shape of the electric fields in the absence of the sample. The two calibration constants in the formula,  $A$  and  $F_{sh}$  can be determined either by comparison with known samples or with computer simulations. The absolute calibration is normally performed at room temperature and uses measurements

on known high purity standards. For solid samples, single crystal high-purity sapphire is utilized as a standard with  $\epsilon'_r = 11.54$  with the electric field parallel to the C-axis and  $\epsilon'_r = 9.34$  with the electric field perpendicular to the C-axis. Furthermore, Teflon with  $\epsilon'_r = 2.07$  can also be used as a standard at low dielectric constant values.

## RESULTS AND DISCUSSION

### *Thermogravimetric Analysis (TGA) and Derivative Thermogravimetric Analysis (DTGA)*

The thermogravimetric (TGA) data and the corresponding derivative thermogravimetric (DTGA) curve for goethite are shown from room temperature to 1000°C at the heating rate of 7.5°C/min in Figure 2. There is a very small increase in the moisture content of about 0.11%, from room temperature up to about 50°C and it has been shown previously that goethite can absorb some hydroxyl units from the atmosphere (19). The dehydroxylation of goethite occurs in three stages. In Stage I, goethite shows a slow rate of water loss up to about 250°C. In the range between 250°C and 400°C, termed Stage II, there is a peak in the DTGA curve, during the main part of the goethite to hematite dehydroxylation reaction. Being a thermally activated reaction, the temperature range over which the main reaction occurs would be expected to be dependent on the heating rate. The rate of mass change increased to a maximum of about 1.05 %/min (0.14 %/°C) at a temperature of about 370°C. After the maximum, the rate of dehydration began to decrease until the reaction was essentially completed at about 400°C. In Stage III, at temperatures above 400°C, the evolution rate is reduced but water continues to be liberated although at a diminishing rate, even up to 1000°C. The theoretical mass loss according to equation (1) would be 10.1 mass percent and this is approximately the value obtained in the present experiments as shown in Figure 2.

### *Real ( $\epsilon'$ ) and Imaginary Permittivities ( $\epsilon''$ )*

The real ( $\epsilon'$ ) and the imaginary permittivities ( $\epsilon''$ ) of goethite are shown as a function of both temperature and frequency in the three dimensional mesh plots in Figure 3 (a) and Figure 3 (b), respectively. In general, the real and the imaginary permittivities follow similar trends. The real permittivities are relatively constant at temperatures below 300°C and at high frequencies. The imaginary permittivities are also constant but their values are significantly lower than the real permittivities and are only slightly above zero at temperatures below 300°C. During the goethite to hematite transition there is a significant peak in both the real and the imaginary permittivities. After the transformation and above about 500°C, both the permittivities increased rapidly with temperature. Also, it can be noted that both the real and the imaginary permittivities increased with decreasing frequency. The relative changes in the imaginary permittivities, as a function of frequency and in particular temperature, are much larger than those for the real permittivities. On cooling, the dielectric data was irreversible and there was no peak.

Figure 4 shows the real and the imaginary permittivities up to almost 1000°C at a frequency of 2460 MHz, which is the frequency used in most microwave applications. From 24°C to about 100°C there was a slight increase in  $\epsilon'$  and this is likely due to the evaporation of a small amount of free water, which results in some mass loss and an increase in the sample density. Above 100°C, the  $\epsilon'$  values decreased slightly, then remained essentially constant and at about 200°C began to increase somewhat with temperature up to about 330°C. Overall, the real permittivity increased only marginally from room temperature to 330°C and the average value of  $\epsilon'$  was 7.77. On the other hand, the imaginary permittivities were low and had an average value of about 0.08 over the

same temperature range. At about 300°C, as the goethite started to convert to hematite, both  $\epsilon'$  and  $\epsilon''$  increased and reached peak values at 380°C of 13.31 and 7.85, respectively. During the dehydroxylation process, the relative change in  $\epsilon''$  was significantly larger than that for  $\epsilon'$ . Beyond the maximum, both  $\epsilon'$  and  $\epsilon''$  decreased and  $\epsilon'$  had an average value of 7.37 from about 425°C to 625°C. This value of the real permittivity ( $\epsilon'$ ) is slightly lower than the average value of 7.77 for temperatures below 325°C, suggesting a loss of material, as would be expected if water was evolved from the mineral with no volume change. From about 650°C to 800°C, the values of  $\epsilon'$  and  $\epsilon''$  began to increase with the relative increase in  $\epsilon''$  being again significantly larger than  $\epsilon'$ . Excluding the goethite to hematite transition, the  $\epsilon'$  values for goethite were found to vary with temperature according to the following equation with a correlation coefficient ( $R^2$ ) of 0.998:

$$\epsilon' = 7.78 - 1.2 \times 10^{-3}T - 5.0 \times 10^{-6}T^2 + 2.0 \times 10^{-7}T^3 - 7.0 \times 10^{-10}T^4 + 1.0 \times 10^{-12}T^5 - 5.0 \times 10^{-16}T^6 \quad (9)$$

Similarly, excluding the goethite to hematite transition, the imaginary permittivity was found to vary with temperature as follows with a correlation coefficient ( $R^2$ ) of 0.999:

$$\epsilon'' = 0.409 - 1.19 \times 10^{-2}T + 1.0 \times 10^{-4}T^2 - 2.0 \times 10^{-7}T^3 + 5.0 \times 10^{-11}T^4 + 4.0 \times 10^{-13}T^5 - 3.0 \times 10^{-16}T^6 \quad (10)$$

It is noteworthy that at the higher temperatures, the curves for  $\epsilon'$  and  $\epsilon''$  are essentially parallel in Figure 4 and this is reflected in the similarity of the higher order terms in equations (9) and (10).

The real permittivities ( $\epsilon'$ ) of the mineral goethite ( $\alpha\text{-FeO}\cdot(\text{OH})$ ) are shown as a function of temperature up to about 650°C at six different frequencies in the range of 397 MHz to 2986 MHz in Figure 5. Below about 330°C, the values of  $\epsilon'$  were essentially independent of frequency, except for the slightly higher values at 2460 MHz. As

mentioned previously, at low temperatures the value of  $\epsilon'$  is mainly determined by charge polarization which is very fast and thus frequency independent. The slightly higher values at 2460 MHz may reflect the increased interaction of the microwaves with the hydrated water in the mineral at that particular frequency. However, this relatively minor effect is smaller than the 2% error of the measurements.

Above about 330°C, as the goethite began to convert to hematite,  $\epsilon'$  increased rapidly and reached a maximum value of 10.88 at a frequency of 397 MHz at about 380°C as shown in Figure 5. For each frequency, the magnitude of the peak decreased with increasing frequency. Also it can be noted that the frequency dependency was more significant at the lower frequencies. The temperature range of the peak corresponds to the dehydroxylation temperature range of goethite, as shown in Figure 2, and thus the increase in the real permittivity is due to the movement of ions during the dehydroxylation process.

Figure 6 shows the peak values of the real permittivity as a function of frequency for the two different heating rates of 3.2°C/min and 7.5°C/min. The experimental results at a heating rate of 3.2°C/min were fitted to an inverse first order polynomial with a correlation coefficient ( $R^2$ ) of 0.999 as follows:

$$\epsilon'_{\text{peak}} = 7.95 + \frac{1.17 \times 10^3}{f} \quad (11)$$

where  $f$  is the frequency in MHz. It is clear from Figure 6, that the magnitude of the peak real permittivity is a strong function of not only frequency but also the heating rate. The goethite to hematite transformation is a relatively slow endothermic reaction and the transformation temperature range is dependent on the heating rate. Slower heating rates allow more time for the dehydroxylation reaction to occur between the permittivity

measurements, more water has previously been evolved and thus the rate of ion generation is reduced at each temperature. This will result in lower permittivities during the transformation process and a lower temperature for the peak permittivity value.

After the peak at 380°C, the real permittivities decreased rapidly and as shown in Figure 5 there was also a step change as the  $\epsilon'$  values fell below those at 330°C. As mentioned previously, the value of  $\epsilon'$  is mainly determined by charge polarization and therefore the step decrease can be attributed to the reduction in the number of atoms per unit volume as the water is evolved and the goethite is converted to hematite. During the measurements there was no change in the bulk sample volume and the actual bulk sample density decreased during the run, from an initial value of 3.08 gm/cc to 2.75 gm/cc after the full heating and cooling cycle. Goethite and hematite have single crystal densities of 4.1 g/cc and 5.3 g/cc, respectively.

Figure 7 shows an enlarged view of Figure 5 over the temperature range from 400°C to 650°C. It can be seen that after the thermal transformation and above 406°C the frequency dependency of the real permittivity again was small and the average value of 7.31 was similar to that exhibited below 330°C. However, as the temperature increased above 406°C, the real permittivity increased more rapidly at the lower frequencies than at the higher frequencies. The temperature range of about 400 to 600°C, over which this effect occurred, will be referred to as the frequency inversion transition region. At temperatures above this region, the frequency dependency becomes the same as during the transformation.

Kryukova et al showed that the hematite which forms from goethite at 400°C contains two percent hydroxyl groups (25). Also the hematite which was produced at 400°C had

close orientation relationships with the original goethite and the crystal morphology did not change during the dehydroxylation process. At 400°C narrow voids were observed, these formed closed spherical pores at 500°C and the hydroxyl groups disappeared at 600°C. The temperature range from 400°C to 600°C is the range over which hydrohematite is converted into hematite (11). Therefore, the inversion in the frequency dependency from 400 to 600°C, as shown in Figure 7, may reflect both the structural modifications and also the changes which occur as the residual hydroxyl groups are removed from the dehydroxylated goethite.

Figure 8 shows the effect of temperature on the imaginary permittivities ( $\epsilon''$ ) at the six different frequencies and the general shapes of the curves were similar to those observed for the real permittivities as shown in Figure 5. Although the values of  $\epsilon''$  were much lower than  $\epsilon'$ , the relative changes in  $\epsilon''$  were significantly larger than those for  $\epsilon'$ . While there was a significant peak during the transformation of goethite to hematite, the values of  $\epsilon''$  below 305°C were less than about 0.2 and therefore the step was non-existent at low frequencies and very small at high frequencies. In a manner similar to the real permittivities, the imaginary permittivity was essentially independent of temperature below the transformation. Furthermore, both during and after the transformation, the values of the imaginary permittivity increased with increasing frequency under all conditions. However, there was no frequency transition region as was observed for the real permittivity.

The peak imaginary permittivities ( $\epsilon''_{\text{peak}}$ ) at 380°C for the two heating rates of 3.2°C/min and 7.5°C/min were plotted as a function of frequency in Figure 9 and it can be seen that the frequency dependency decreased with increasing frequency. The peak

values at the heating rate of 3.2°C/min were fitted to an inverse second order polynomial equation with a correlation coefficient ( $R^2$ ) of 0.999 as follows:

$$\varepsilon''_{\text{peak}} = 0.50 + \frac{3.25 \times 10^3}{f} - \frac{4.48 \times 10^3}{f^2} \quad (12)$$

where  $f$  is the frequency in MHz. Attempting to fit the data to an inverse first order polynomial gave a relatively poor fit, which indicates that the relationship between  $\varepsilon''$  and frequency is more complex than that between  $\varepsilon'$  and frequency. Higher heating rates result in significant increases in the complex permittivities. However, in comparison to the real permittivities, the relative increases in the complex permittivities are much larger as the heating rate increases from 3.2°C/min to 7.5°C/min. This reflects the stronger dependency of the complex permittivity on both the number and the rate of movement of ions.

#### *Loss Tangent ( $\tan\delta$ )*

The loss tangent ( $\tan\delta$ ) of goethite is shown as a function of both temperature and frequency in the three dimensional mesh plot in Figure 10. It can be seen that the loss tangent followed trends similar to the real and imaginary permittivities. At temperatures below about 305°C, the loss tangent values were low, essentially independent of frequency and varied from about 0.08 to 0.017. However, as the goethite began to dehydroxylate the loss tangent increased rapidly, particularly at low frequencies and the peak loss tangent ( $\tan\delta_{\text{peak}}$ ) increased with decreasing frequency. After the reaction was complete and at about 406°C, the loss tangent dropped again to a low value and then began to increase rapidly with temperature. Above 406°C, the loss tangent increased with decreasing frequency and this effect was more pronounced at the lower frequencies.

#### *Comparison of the DTGA with the Real ( $\varepsilon'$ ) and Imaginary ( $\varepsilon''$ ) Permittivities*

Figure 11 provides a comparison of the DTGA curve for goethite with both the real ( $\epsilon'$ ) and the imaginary permittivities ( $\epsilon''$ ) at 2460 MHz. It can be seen that the changes in the permittivities during the goethite to hematite transformation were a strong function of the changes in the combined moisture content. Both  $\epsilon'$  and  $\epsilon''$  increased with the rate of water removal and vice versa during the thermal transformation of goethite to hematite, with the effect being more significant for  $\epsilon''$  than for  $\epsilon'$ . A number of researchers have shown that for thermal decomposition reactions there is a correlation between the dielectric properties of a material and the Derivative Thermogravimetric Analysis (DTGA) data or Differential Thermal Analysis (DTA) data (26-33). The relationship between the permittivities ( $\epsilon'$  and  $\epsilon''$ ) and the rate of change of water content (DTGA) during the conversion of goethite to hematite can be explained in terms of the liberation of hydroxyl units and the formation of water vapour and oxygen ions according to the following reaction:



When the rate of water removal is high, the flux of migrating hydroxyl units will be high and this will result in an increase in the permittivities. After the maximum flux of hydroxyl ions, which corresponds to the maximum rate of water removal, the permittivities will decrease. As mentioned previously, the hematite, which is formed from the dehydroxylation of goethite contains residual hydroxyl units and is called hydrohematite. Thus, the dielectric properties of the hydrohematite produced from goethite should be different from hematite, which does not contain any residual hydroxyl ions. Also Kryukova et al have shown that at 600°C the hematite structure consisted of slightly misoriented crystalline blocks (25). A dislocation network formed at 700°C and

from 800°C to 1000°C, the dislocations disappeared with the simultaneous formation of twins and macrosteps due to the recrystallization process. Therefore, as shown in Figure 12, above the goethite to hematite transition, the values of  $\epsilon'$  and  $\epsilon''$  are higher for the defected hematite produced from goethite, than those of the mineral hematite, which does not contain these residual hydroxyl units and/or defects.

#### *Relaxation Times ( $\tau$ )*

A plot on rectangular coordinates of  $\epsilon''$  versus  $\epsilon'$  at various temperatures is shown in Figure 13. The data have been divided into three regimes as discussed previously; Stage I, which are temperatures below the goethite to hematite transition; Stage II, which are temperatures in the main goethite to hematite transformation temperature range; and Stage III, which are temperatures above the main goethite to hematite transition. For temperatures before the reaction, i.e. below 305°C, the values of the imaginary permittivity are very low and essentially independent of temperature and frequency. During the reaction, i.e. for temperatures from 330°C to 380°C, both  $\epsilon'$  and  $\epsilon''$  increase, as ions are generated during the dehydroxylation process. As mentioned previously, the relative increase in  $\epsilon''$  is larger than that of  $\epsilon'$ , since  $\epsilon''$  is more sensitive to processes which involve the movement of ions. The values of  $\epsilon'_{\infty}$ , i.e. the high frequency limiting values of  $\epsilon'$ , during the reaction are similar to the values before the reaction. After the reaction, at temperatures in the range of 406°C to 630°C, the majority of the experimental points fall on a common curve with a common value of  $\epsilon'_{\infty}$ . A comparison of the Debye relationships as given in equations (3) and (4) yields:

$$\epsilon' = \epsilon'_s - \tau(\omega\epsilon'') \quad (14)$$

and

$$\varepsilon' = \varepsilon'_{\infty} + \left( \frac{\varepsilon''}{\omega} \right) \frac{1}{\tau} \quad (15)$$

According to equation 15, if the Debye relation is obeyed then a linear relationship will be obtained between  $\varepsilon'$  and  $(\varepsilon''/\omega)$  and the slope of the plot will be linear with a value of  $(1/\tau)$ . Figures 14 (a) and 14 (b) show the  $\varepsilon'$  versus  $(\varepsilon''/\omega)$  plots for temperatures during the reaction and after the reaction, respectively. During the conversion of goethite to hematite,  $\varepsilon'$  was not a linear function of  $(\varepsilon''/\omega)$  and thus the Debye equation was not followed. This indicates that there is more than one relaxation time, which would be expected since migrating hydroxyl, oxygen ions and possible hydrogen atoms are involved in the dehydroxylation process. After the reaction from 406°C to 456°C the plots were again non-linear, again reflecting the changing frequency dependency in this transition region. However, above about 500°C, a linear behaviour was observed and as the temperature increased the slope increased, which corresponds to a decrease in the relaxation time,  $\tau$ . This linear behaviour demonstrates that the Debye relationship is being closely followed and there is one relaxation process with a well-defined relaxation time.

Using the theory of absolute reaction rates in condensed phases (34), Eyring has shown that the following equation can be utilized to describe the relaxation behaviour (35):

$$\ln \tau = \frac{\Delta H}{RT} - \ln T + \left( \ln \frac{h}{k} - \frac{\Delta S}{R} \right) \quad (16)$$

where  $\Delta H$  is the activation energy of dipole or ionic relaxation,  $R$  is the gas constant,  $T$  is the temperature,  $h$  is Planck's constant,  $k$  is Boltzman's constant and  $\Delta S$  is the entropy of activation. The last term is independent of temperature and also the  $\ln T$  term is relatively small. Therefore, the slope of an Arrhenius plot of  $\ln \tau$  versus  $1/T$  is  $\Delta H/R$ . Figure 15

shows an Arrhenius plot of the relaxation times,  $\tau$ , which could be calculated after the reaction and after the transition period (507°C to 630°C) from the linear behaviour observed in Figure 14 (b). As mentioned previously,  $\tau$  values could not be obtained for temperatures in the range of 406°C to 481°C, which are after the reaction but during the transition period. Above 507°C the activation energy had a relatively low value of 0.47 kJ/mole.

## CONCLUSIONS

The real and imaginary permittivities and the loss tangent of goethite were determined from room temperature to about 800°C and from 400 MHz to 3000 MHz. Below about 300°C the permittivities were essentially independent of frequency and temperature. Above 300°C and during the goethite to hematite transformation temperature range, the dielectric properties increased with the rate of dehydroxylation and a peak was observed in the dielectric properties. Also, as the sample heating rate increased, the dehydroxylation rate increased and thus the dielectric properties increased even further. The real permittivity decreased with increasing frequency both during and after the transformation, except for a frequency transition range from about 406°C to 456°C where the frequency dependency reversed. This behaviour could indicate that the goethite has been converted to hydrohematite rather than hematite. The imaginary permittivity increased with decreasing frequency and showed no frequency transition region. In addition, the imaginary permittivity was more strongly dependent on frequency than the real permittivity. The dielectric properties of the reacted goethite, i.e. hydrohematite were higher than those of hematite, at the same temperature and this provided further evidence that the hydroxyl ions make a significant contribution to the

dielectric behaviour. Using the Debye formalism, relaxation plots were determined both during and after the main goethite to hematite reaction. The relaxation times were non-linear both during the main reaction and also during the transition period after the reaction. However, linear behaviour was observed above about 500°C. This behaviour of the relaxation times again indicates that hydrohematite exists after the main goethite to hematite reaction. The Arrhenius equation for thermally activated relaxation times was used to calculate the activation energy above about 500°C and a value of 0.47 kJ/mole was obtained.

## ACKNOWLEDGEMENTS

The authors would like to thank the Natural Sciences and Engineering Research Council of Canada, the Center for Chemical Process Metallurgy (C-CPM) and Microwave Properties North (MPN) for their support of this research. Also we would like to express our gratitude to H. Frank Gibbs of the Brockhouse Institute for Materials Research at McMaster University for the Thermogravimetric Analysis work.

## REFERENCES

1. W. C. Sleppy, "Alumina and Aluminum", in Ullmann's Encyclopedia of Chemical Technology, Edited by J. I. Kroschwitz and M. Howe-Craft, Fourth Edition, John Wiley and Sons, Vol. 2, 1992, pp. 252-256.
2. K. Wefers, "Bauxite, the Principal Raw Material", in Handbook of Extractive Metallurgy, Edited by F. Habashi, Wiley-VCH, Vol. II, Chapter 21, 1997, pp.1068-1072.
3. M. Novotny, Z. Solc and M. Trojan, "Pigments" in Ullmann's Encyclopedia of Chemical Technology, Edited by J. I. Kroschwitz and M. Howe-Craft, Fourth

- Edition, John Wiley and Sons, Vol. 19, 1992, pp. 1-40.
4. G. Bate, in *Magnetic Oxides, Part 2*, Edited by D. J. Craik, Wiley and Sons, New York, 1975, p.689.
  5. H. Kathrein and L. Leitner, "Iron Magnetic Pigments", in *Handbook of Extractive Metallurgy*, Edited by F. Habashi, Wiley-VCH, Vol. I-Part II: Chapter 5-Ferrous Alloys, Section 5.21.3, 1997, pp. 1068-1072.
  6. E. Wolska and U. Schwertmann, "Nonstoichiometric Structures During Dehydroxylation of Goethite", *Zeitschrift fuer Kristallographie*, Vol. 189 (3-4), 1989, pp. 223-237.
  7. E. Wolska and W. Szajda, "Structural and Spectroscopic Characteristics of Synthetic Hydrohematite", *Journal of Materials Science*, 20, 1985, pp. 4407-4412.
  8. E. Wolska, "The Structure of Hydrohematite", *Zeitschrift fuer Kristallographie*, Vol. 154, 1981, pp. 69-75.
  9. E. Wolska, "Relations Between the Existence of Hydroxyl Ions in the Anionic Sublattice of Hematite and its Infrared and X-ray Characteristics", *Solid State Ionics*, Vol. 28-30, 1988, pp. 1349-1351.
  10. S. Yariv and E. Mendelovici, "The Effect of Degree of Crystallinity on the Infrared Spectrum of Hematite", *Appl. Spectrosc.*, Vol. 33, 1979, pp. 410-411.
  11. G. F. Huttig and E. Strotzer, "Die Aktiven Zustände, Welche im Verlaufe des Zersetzung des Nadeleisenerzes in  $\alpha$ -Eisenoxyd und Wasserdampf Durchschritten Werden", *Z. Anorg. Allg. Chem.*, Vol. 226, 1936, pp. 97-125.
  12. F. Watari, P. Delavignette J. von Landuyt, and S. Amelinckx, "Electron

- Microscopy Study of Dehydration Transformation. Part III: High Resolution Observation of the Reaction Process  $\text{FeOOH} \rightarrow \text{Fe}_2\text{O}_3$ ”, *J. Solid State Chem.*, Vol. 48, 1983, pp. 49-64.
13. D. Walter, G. Buxbaum and W. Laqua, “The Mechanism of the Thermal Transformation from Goethite to Hematite”, *Journal of Thermal Analysis and Calorimetry*, Vol. 63, 2001, pp. 733-748.
  14. R. C. Mackenzie, and G. Berggren, In *Differential Thermal Analysis 1*, Academic Press, 1970, pp. 271-302.
  15. M. B. Fey and J. B. Dixon, “Synthesis and Properties of Poorly Crystalline Hydrated Aluminous Goethites”, *Clays and Clay Minerals*, 29, 1981, pp. 91-100.
  16. D. G. Schulze, and U. Schwertmann, “The Influence of Aluminum on Iron Oxides: X. Properties of Aluminum-Substituted Goethites”, *Clay Minerals*, 19 (4), 1984, pp. 521-539.
  17. C. J. Goss, “The Kinetics and Reaction Mechanism of the Goethite to Hematite Transformation”, *Minerals Magazine*, 51, 1987, pp. 437-451.
  18. H. D. Ruan and R. J. Gilkes, “Dehydroxylation of Aluminous Goethite: Unit Cell Dimensions, Crystal Size and Surface Area”, *Clays and Clay Minerals*, 43 (2), 1995, pp. 196-211.
  19. H. D. Ruan, R. L. Frost, J. T. Kloprogge and L. Duong, “Infrared Spectroscopy of Goethite Dehydroxylation: III FT-IR Microscopy of In Situ Study of the Thermal Transformation of Goethite To Hematite”, *Spectrochimica Acta, Part A: Molecular and Biomolecular Spectroscopy*, 58A (5), 2002, pp. 967-981.
  20. H. D. Ruan and R. J. Gilkes, “Dehydroxylation of Aluminous Goethite: Unit Cell

- Dimensions, Crystal Size and Surface Area”, *Clays and Clay Minerals*, 43 (2), 1995, pp. 196-211.
21. H. Stanjek and U. Schwertmann, “The Influence of Aluminum on Iron Oxides. Part XVI: Hydroxyl and Aluminum Substitution in Synthetic Hematites”, *Clays and Clay Minerals*, 40 (3), 1992, pp. 347–354.
22. G. N. Kustova, E. B. Burgina, V. A. Sadykov, and S. G. Poryvaev, “Vibrational Spectroscopic Investigation of the Goethite Thermal Decomposition Products”, *Physics and Chemistry of Minerals*, 18, 1992, pp. 379-382.
23. R. M. Hutcheon, M. S. De Jong, F. P. Adams, P. G. Lucuta, J. E. McGregor and L. Bahen, “RF and Microwave Dielectric Measurements to 1400°C and Dielectric Loss Mechanisms”, *Materials Research Society Symposium Proceedings, (Microwave Processing of Materials III)*, 269, 1992, pp. 541-551.
24. R. M. Hutcheon, M. S. de Jong and F. P. Adams, “A System for Rapid Measurement of RF and Microwave Properties up to 1400°C”, *Journal of Microwave Power and Electromagnetic Energy*, 27 (2), 1992, pp. 87-92.
25. G. N. Kryukova, S. V. Tsybulya, L. P. Solovyeva, V. A. Sadykov, G. S. Litvak and M. P. Andrianova, “Effect of Heat Treatment on the Microstructure Evolution of Haematite Derived from Synthetic Goethite”, *Materials Science and Engineering*, A149, 1991, pp. 121-127.
26. E. Karmazsin, “Use of Low- and High-Power Microwave Energy for Thermal Analysis”, *Thermochimica Acta*, Vol. 110, 1987, pp. 289-95.
27. E. Karmazsin, R. Barhoumi, P. Satre and F. Gaillard, “Use of Microwaves in Thermal Analysis”, *Journal of Thermal Analysis*, Vol. 30 (1), 1985, pp. 43-47.

28. E. Karmazsin, R. Barhoumi and P. Satre, "Thermal Analysis with Microwaves. Temperature and Power Control", *Journal of Thermal Analysis*, Vol. 29 (6), 1984, pp. 1269-77.
29. G. M. B. Parkes, P. A. Barnes, E. L. Charsley and G. Bond, "Microwave Differential Thermal Analysis in the Investigation of Thermal Transitions in Materials", *Analytical Chemistry*, Vol. 71 (22), 1999, pp. 5026-5032.
30. G. M. B. Parkes, G. Bond, P. A. Barnes and E. L. Charsley, "Development of a New Instrument for Performing Microwave Thermal Analysis", *Review of Scientific Instruments*, Vol. 71(1), 2000, 168-175.
31. G. M. B. Parkes, P. A. Barnes, G. Bond and E. L. Charsley, "Qualitative and Quantitative Aspects of Microwave Thermal Analysis", *Thermochimica Acta*, Vol. 356 (1-2), 2000, pp. 85-96.
32. G. M. B. Parkes, P. A. Barnes, E. L. Charsley and G. Bond, "Microwave Thermal Analysis - A New Approach to the Study of the Thermal and Dielectric Properties of Materials" *Journal of Thermal Analysis and Calorimetry*, Vol. 56 (2), pp. 723-731.
33. R.M. Hutcheon, P. Hayward, B.H. Smith and S.B. Alexander, "High Temperature Dielectric Constant Measurement - Another Analytical Tool for Ceramic Studies", *Microwaves: Theory and Application in Materials Processing III*, *Ceramic Transactions*, American Ceramic Society, Vol. 59, 1995, pp. 235-241.
34. W. F. K. Wynne-Jones and H. Eyring, "The Absolute Rate of Reactions in Condensed Phases", *Journal of Chemical Physics*, Vol. 3, 1935, pp. 492-402.
35. H. Eyring, "Viscosity, Plasticity and Diffusion as Examples of Absolute Reaction

### LIST OF FIGURE CAPTIONS

- FIGURE 1: Schematic diagram of the  $TM_{0n0}$  cavity system (in cross-section) showing the linear actuator with the quartz sample holder and a sample located on axis in the centre of the cavity.
- FIGURE 2: Thermogravimetric Analysis (TGA) data and the corresponding Derivative Thermogravimetric Analysis (DTGA) data for goethite. The heating rate was  $7.5^{\circ}\text{C}/\text{min}$ .
- FIGURE 3 (a): Three dimensional mesh plot of the real permittivity ( $\epsilon'$ ) as a function of temperature and frequency. The heating rate was  $3.2^{\circ}\text{C}/\text{min}$ .
- FIGURE 3 (b): Three dimensional mesh plot of the imaginary permittivity ( $\epsilon''$ ) as a function of temperature and frequency. The heating rate was  $3.2^{\circ}\text{C}/\text{min}$ .
- FIGURE 4: Real ( $\epsilon'$ ) and imaginary permittivities ( $\epsilon''$ ) of goethite from room temperature to  $1000^{\circ}\text{C}$  at a frequency of 2460 MHz. The heating rate was  $7.5^{\circ}\text{C}/\text{min}$ .
- FIGURE 5: Real permittivities ( $\epsilon'$ ) of goethite as a function of temperature at six frequencies. The heating rate was  $3.2^{\circ}\text{C}/\text{min}$ .
- FIGURE 6: Peak values of the real permittivity ( $\epsilon'_{\text{peak}}$ ) at  $380^{\circ}\text{C}$  as a function of frequency for the two heating rates of  $3.2^{\circ}\text{C}/\text{min}$  and  $7.5^{\circ}\text{C}/\text{min}$ .
- FIGURE 7: Enlarged view of Figure 6 over the temperature range from  $400^{\circ}\text{C}$  to  $650^{\circ}\text{C}$ . The heating rate was  $3.2^{\circ}\text{C}/\text{min}$ .
- FIGURE 8: Imaginary permittivities ( $\epsilon''$ ) of goethite as a function of temperature at six frequencies. The heating rate was  $3.2^{\circ}\text{C}/\text{min}$ .
- FIGURE 9: Peak values of the imaginary permittivity ( $\epsilon''_{\text{peak}}$ ) at  $380^{\circ}\text{C}$  as a function of frequency for the two heating rates of  $3.2^{\circ}\text{C}/\text{min}$  and  $7.5^{\circ}\text{C}/\text{min}$ .

FIGURE 10: Three dimensional mesh plot of the loss tangent ( $\tan\delta$ ) as a function of temperature and frequency. The heating rate was  $3.2^{\circ}\text{C}/\text{min}$ .

FIGURE 11: Comparison of the Derivative Thermogravimetric Analysis (DTGA) results with the real ( $\epsilon'$ ) and imaginary permittivities ( $\epsilon''$ ). The heating rate was  $7.5^{\circ}\text{C}/\text{min}$ .

FIGURE 12: Comparison of the real ( $\epsilon'$ ) and imaginary permittivities ( $\epsilon''$ ) of goethite with the mineral hematite. The heating rate was  $7.5^{\circ}\text{C}/\text{min}$ .

FIGURE 13: Plot of the imaginary permittivities ( $\epsilon''$ ) versus the real permittivities ( $\epsilon'$ ) at temperatures, before, during and after the reaction. The heating rate was  $3.2^{\circ}\text{C}/\text{min}$ .

FIGURE 14 (a): Plot of  $\epsilon'$  versus ( $\epsilon''/\omega$ ) for temperatures during the reaction. The heating rate was  $3.2^{\circ}\text{C}/\text{min}$ .

FIGURE 14 (b): Plot of  $\epsilon'$  versus ( $\epsilon''/\omega$ ) for temperatures after the reaction. The heating rate was  $3.2^{\circ}\text{C}/\text{min}$ .

FIGURE 15: Arrhenius plot of ( $\ln \tau$ ) versus  $1/T$  for temperatures after the reaction. The heating rate was  $3.2^{\circ}\text{C}/\text{min}$ .

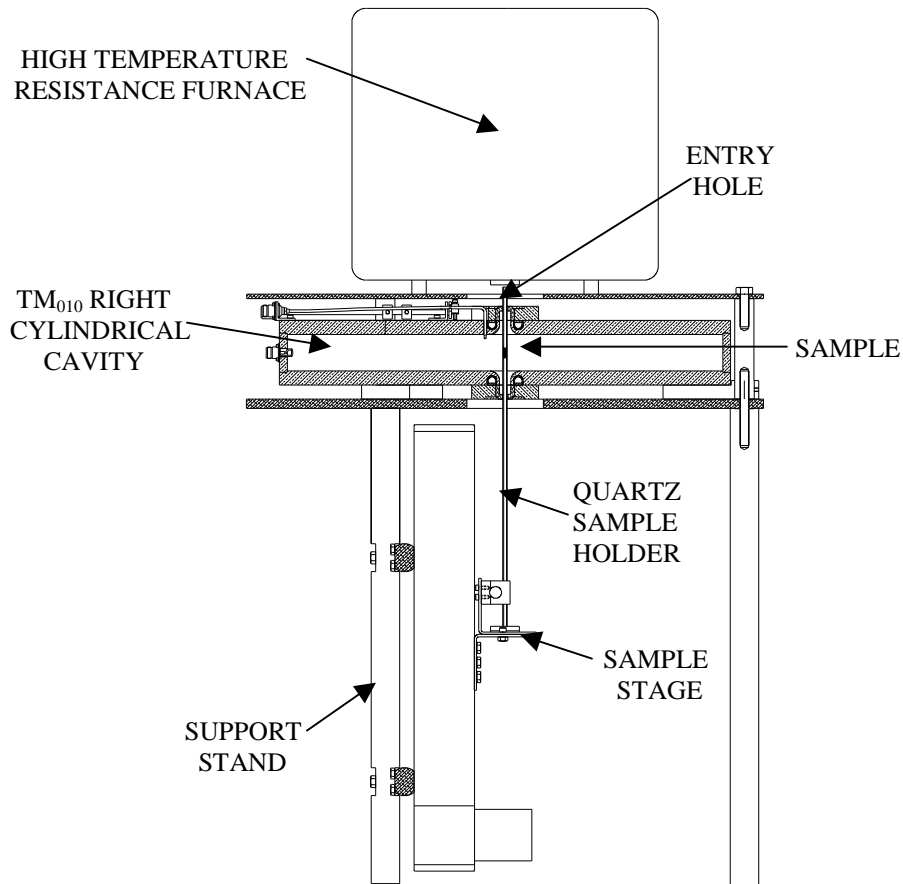


FIGURE 1: Schematic diagram of the  $TM_{0n0}$  cavity system (in cross-section) showing the linear actuator with the quartz sample holder and a sample located on axis in the centre of the cavity.

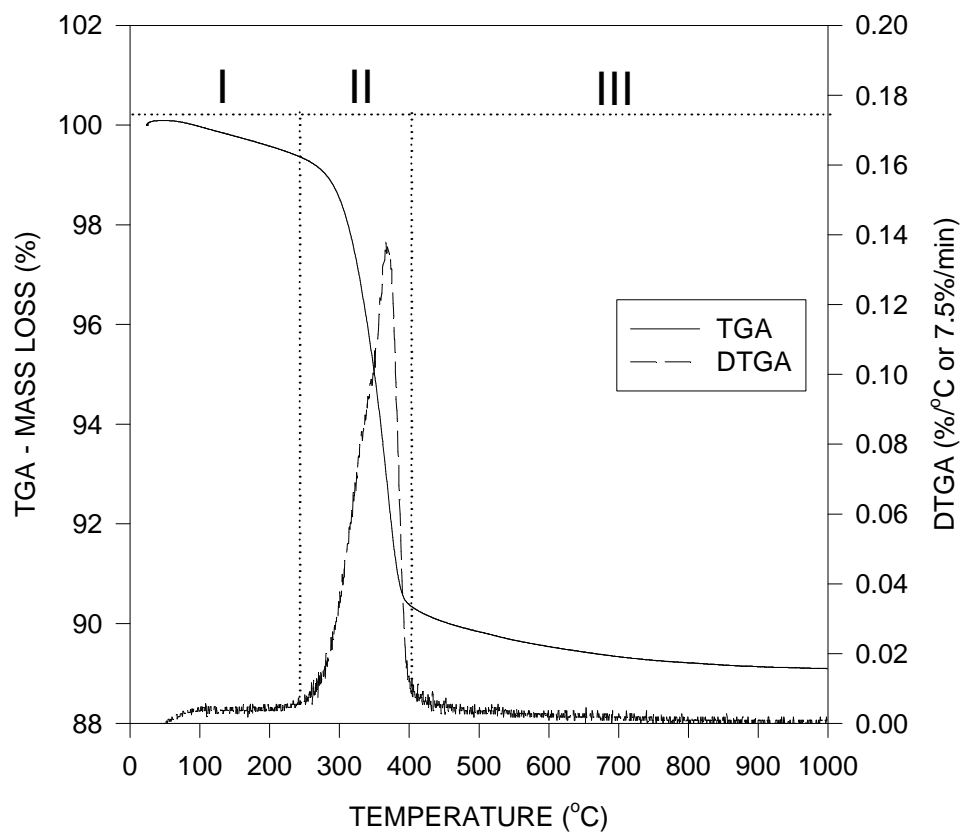


FIGURE 2: Thermogravimetric Analysis (TGA) data and the corresponding Derivative Thermogravimetric Analysis (DTGA) data for goethite. The heating rate was 7.5°C/min.

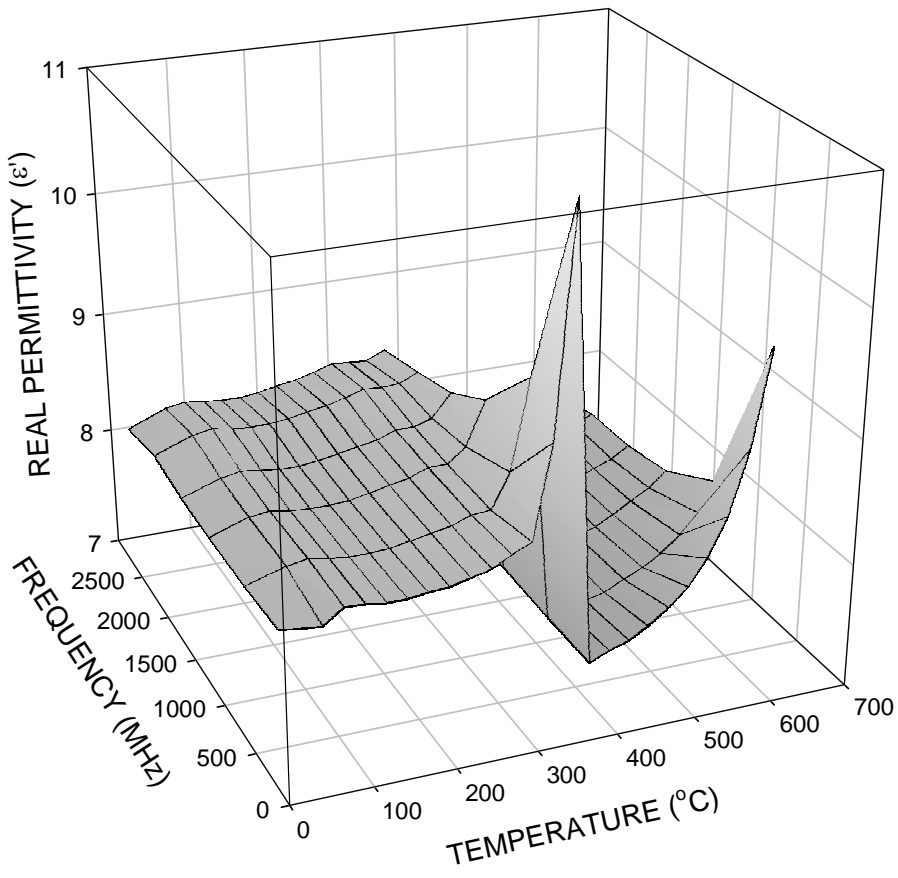


FIGURE 3 (a): Three dimensional mesh plot of the real permittivity ( $\epsilon'$ ) as a function of temperature and frequency. The heating rate was  $3.2^{\circ}\text{C}/\text{min}$ .

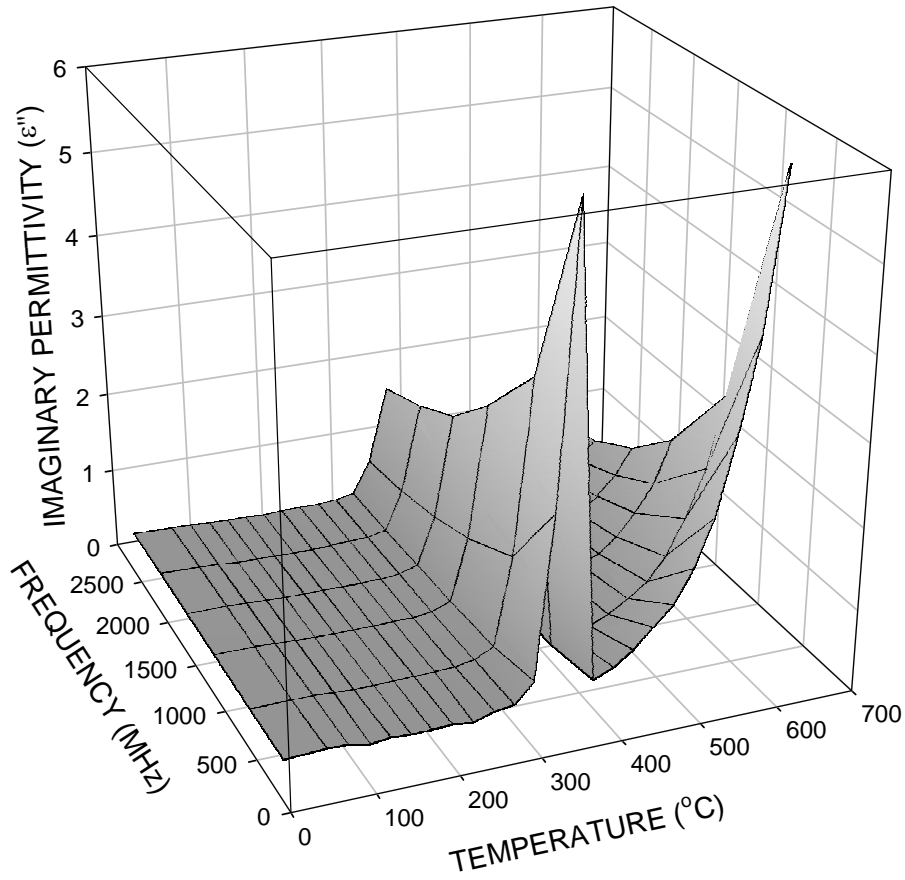


FIGURE 3 (b): Three dimensional mesh plot of the imaginary permittivity ( $\epsilon''$ ) as a function of temperature and frequency. The heating rate was 3.2 $^{\circ}\text{C}/\text{min}$ .

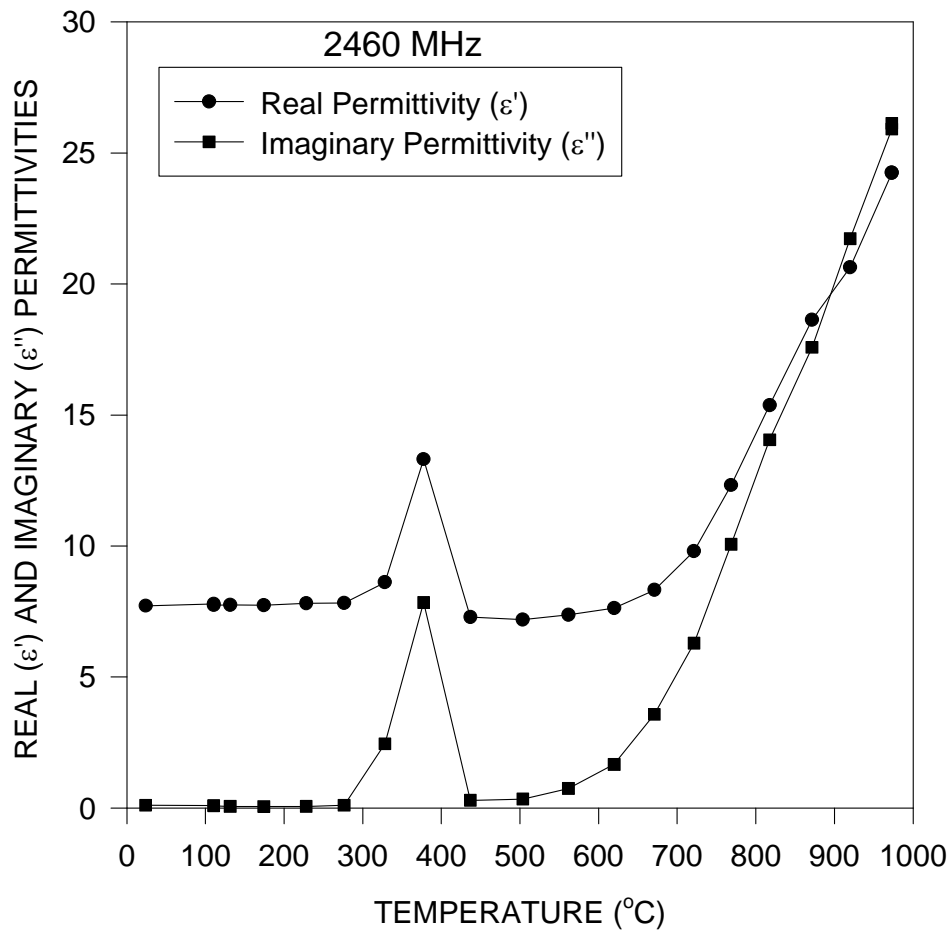


FIGURE 4: Real ( $\epsilon'$ ) and imaginary permittivities ( $\epsilon''$ ) of goethite from room temperature to 1000°C at a frequency of 2460 MHz. The heating rate was 7.5°C/min.

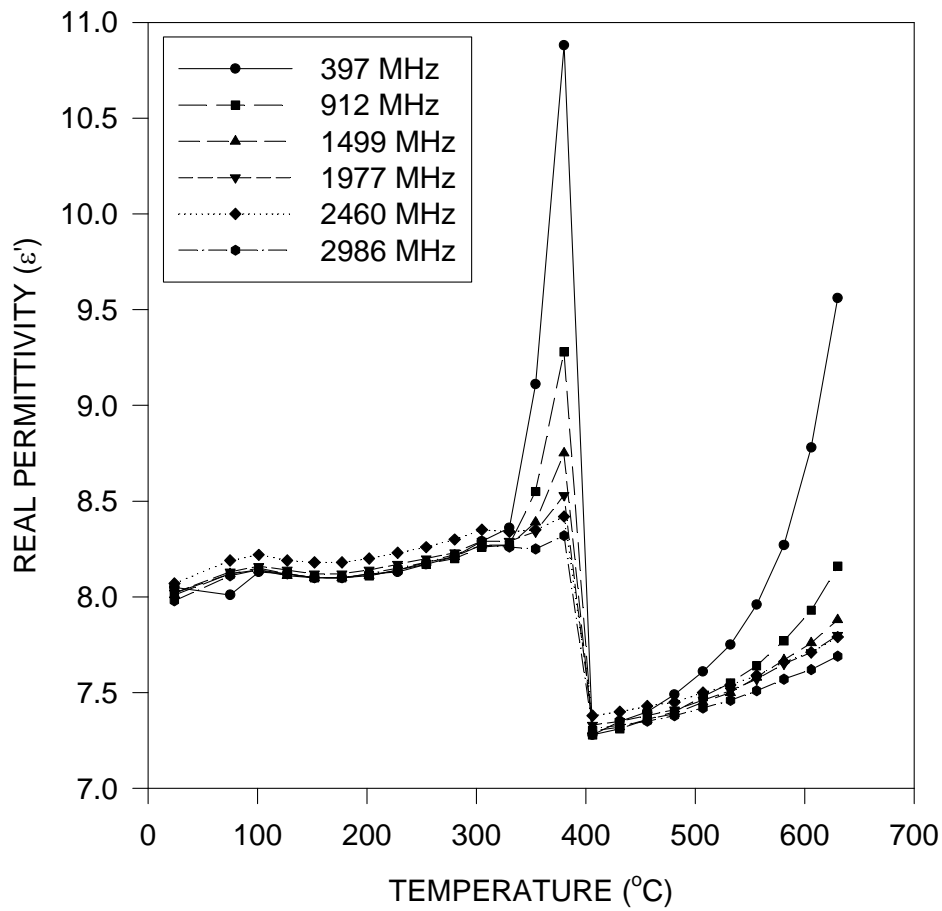


FIGURE 5: Real permittivities ( $\epsilon'$ ) of goethite as a function of temperature at six frequencies. The heating rate was  $3.2^{\circ}\text{C}/\text{min}$ .

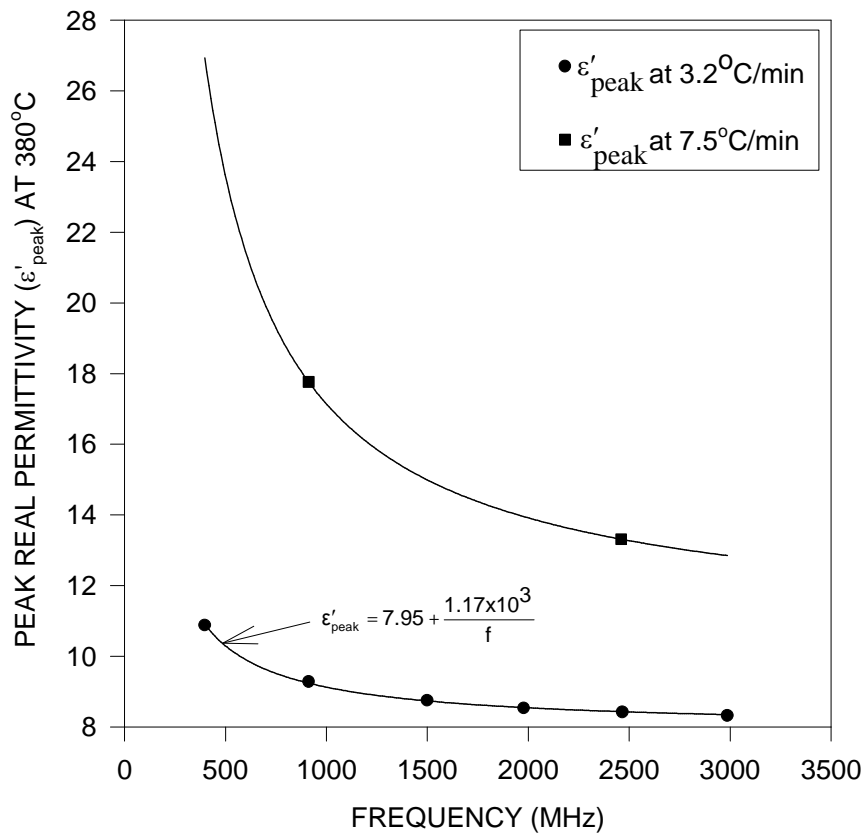


FIGURE 6: Peak values of the real permittivity ( $\epsilon'_{\text{peak}}$ ) at 380°C as a function of frequency for the two heating rates of 3.2°C/min and 7.5°C/min.

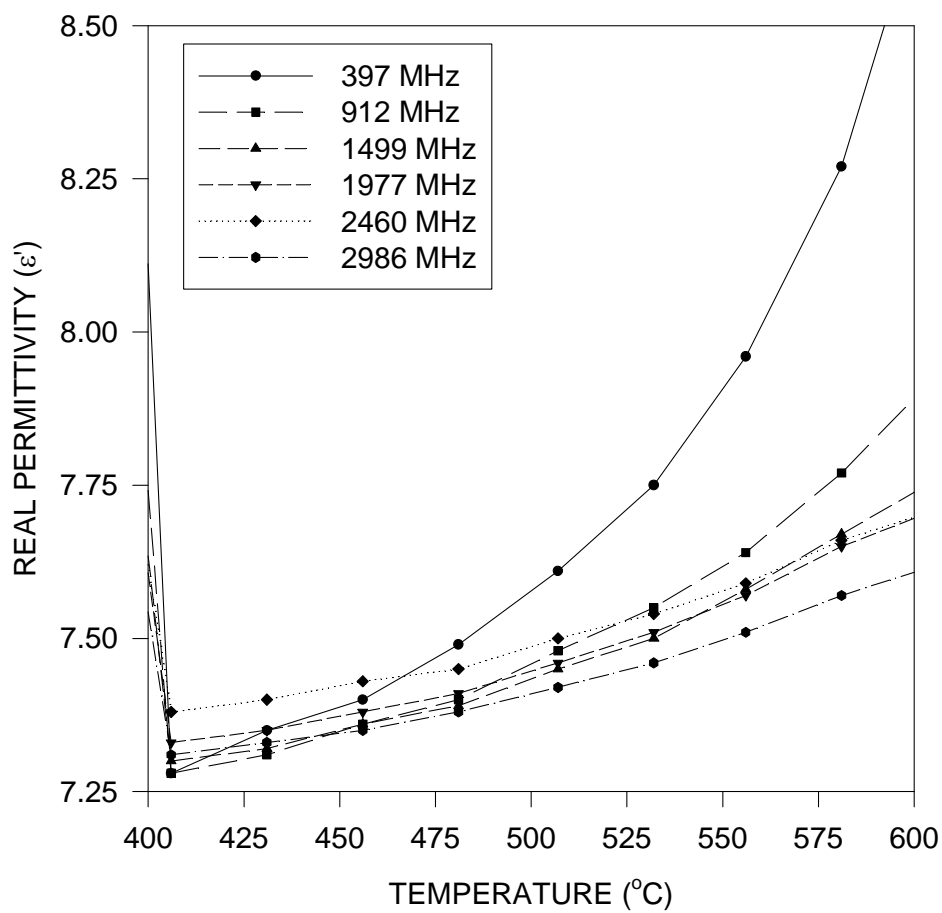


FIGURE 7: Enlarged view of Figure 6 over the temperature range from 400°C to 650°C. The heating rate was 3.2°C/min.

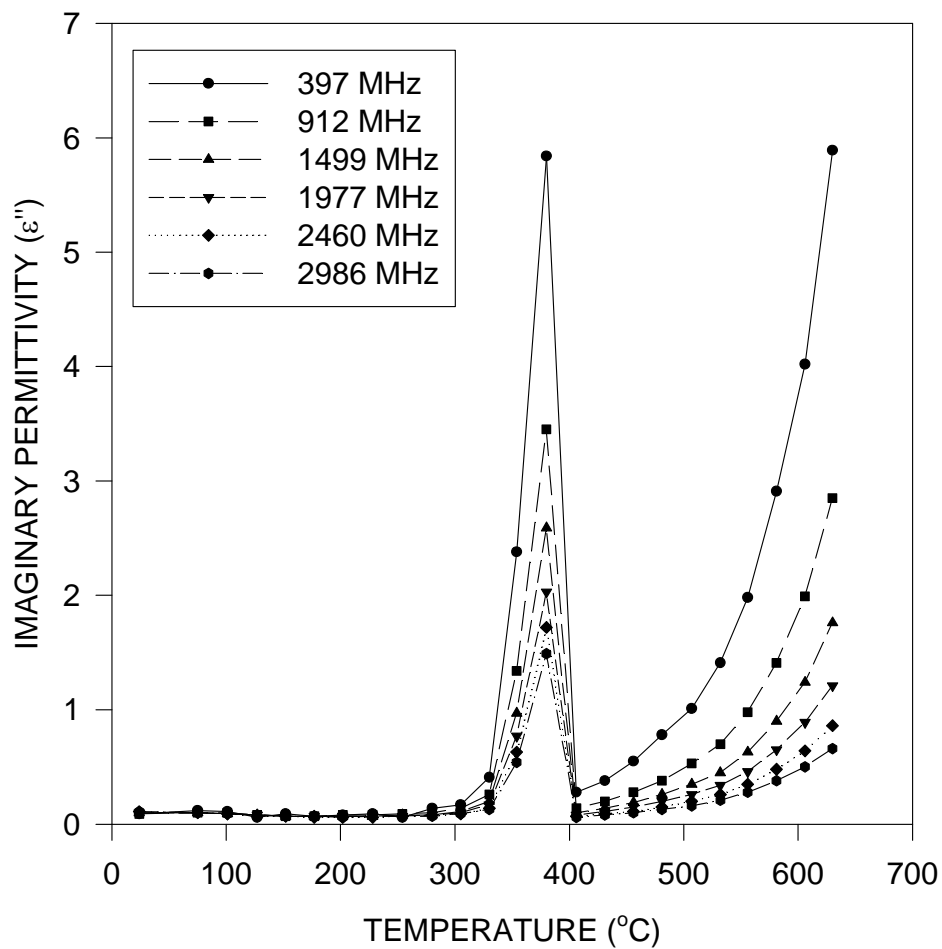


FIGURE 8: Imaginary permittivities ( $\epsilon''$ ) of goethite as a function of temperature at six frequencies. The heating rate was  $3.2^{\circ}\text{C}/\text{min}$ .

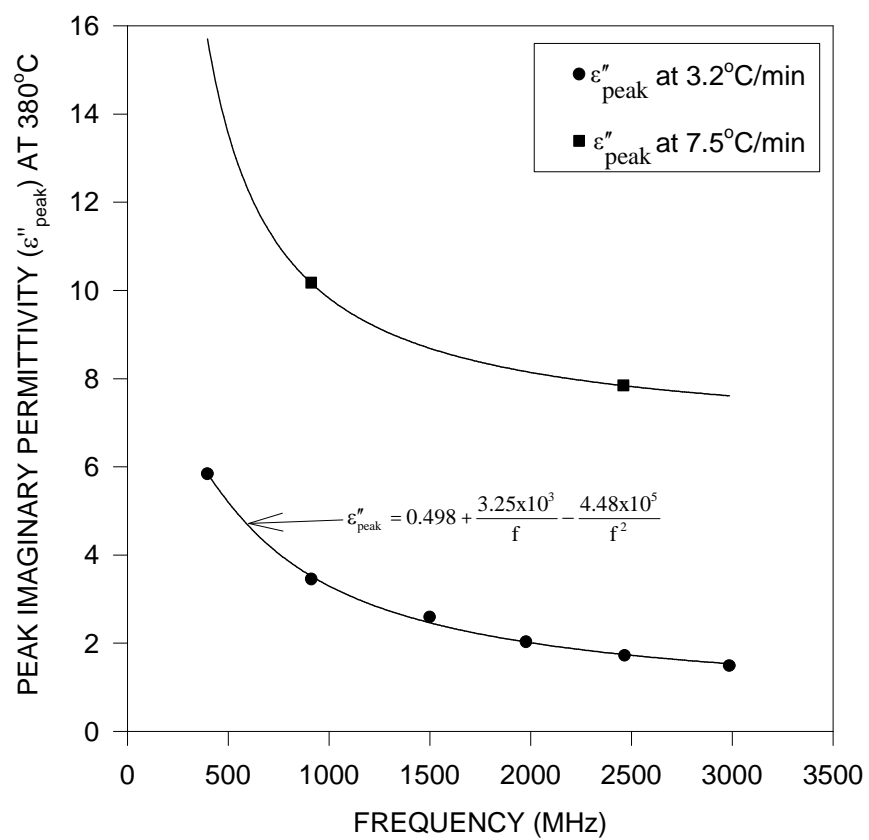


FIGURE 9: Peak values of the imaginary permittivity ( $\epsilon''_{\text{peak}}$ ) at 380°C as a function of frequency for the two heating rates of 3.2°C/min and 7.5°C/min.

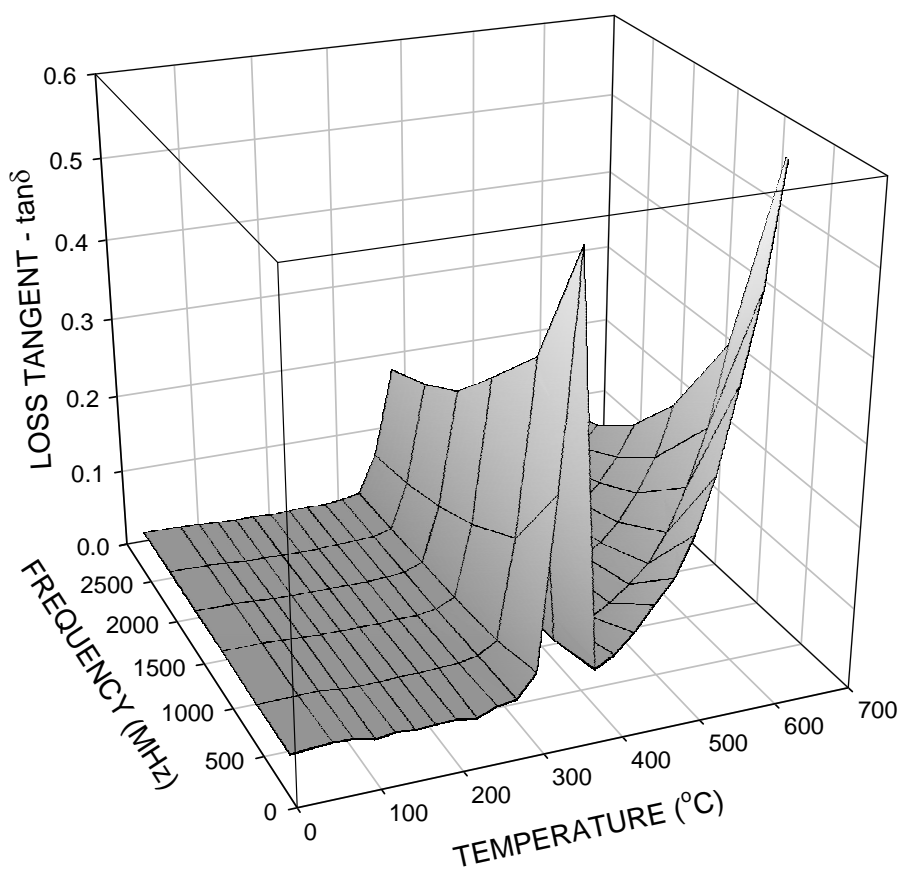


FIGURE 10: Three dimensional mesh plot of the loss tangent ( $\tan\delta$ ) as a function of temperature and frequency. The heating rate was  $3.2^{\circ}\text{C}/\text{min}$ .

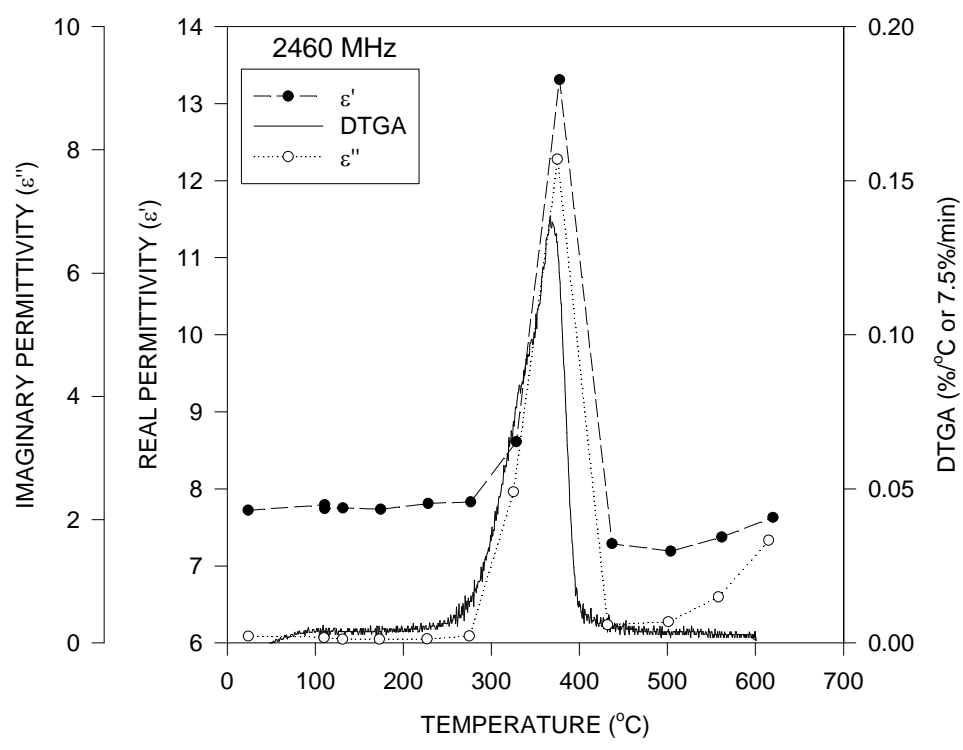


FIGURE 11: Comparison of the Derivative Thermogravimetric Analysis (DTGA) results with the real ( $\epsilon'$ ) and imaginary permittivities ( $\epsilon''$ ). The heating rate was  $7.5^{\circ}\text{C}/\text{min}$ .

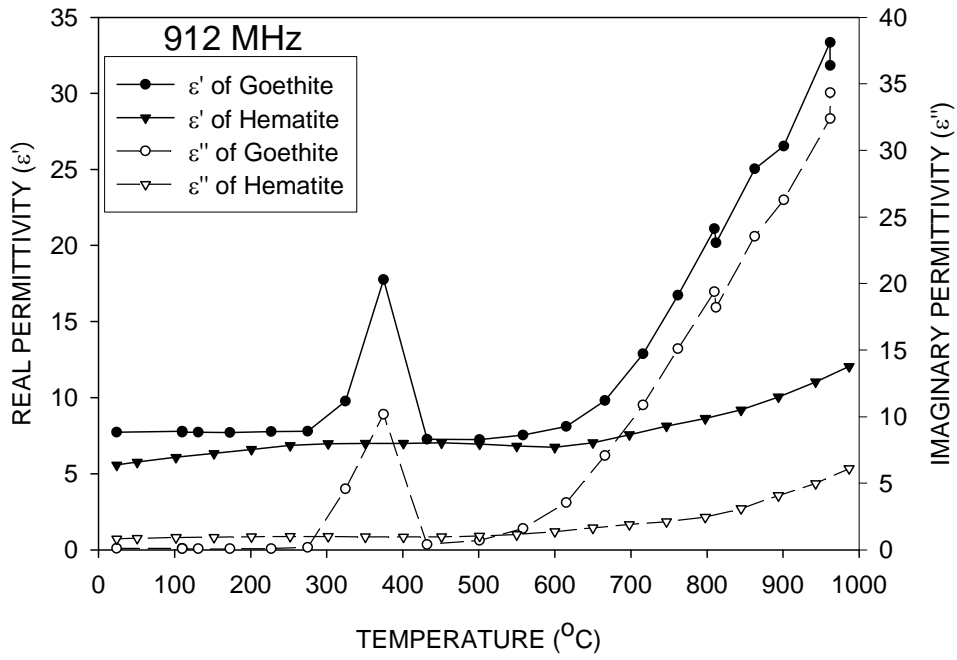


FIGURE 12: Comparison of the real ( $\epsilon'$ ) and imaginary permittivities ( $\epsilon''$ ) of goethite with the mineral hematite. The heating rate was  $7.5^{\circ}\text{C}/\text{min}$ .

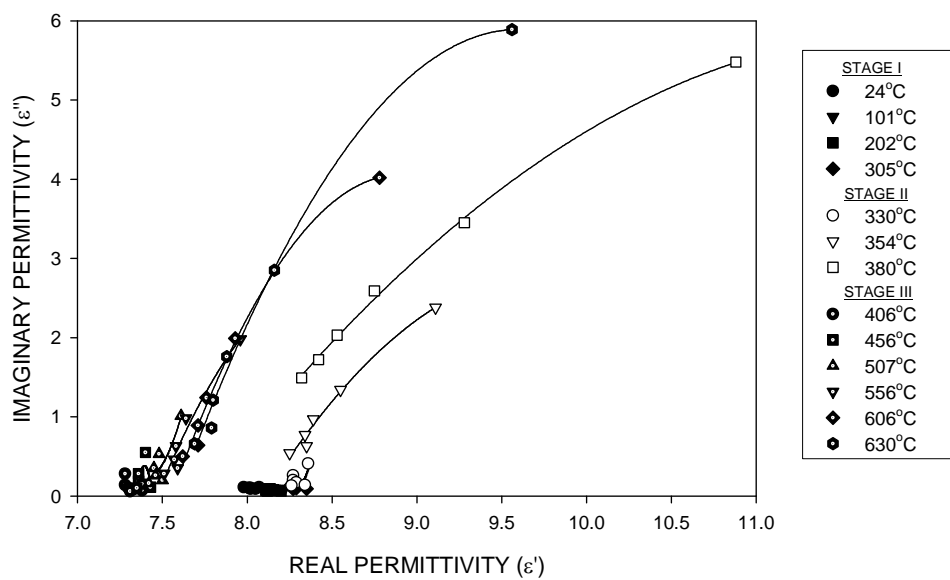


FIGURE 13: Plot of the imaginary permittivities ( $\epsilon''$ ) versus the real ( $\epsilon'$ ) at temperatures, before, during and after the reaction. The heating rate was 3.2°C/min.

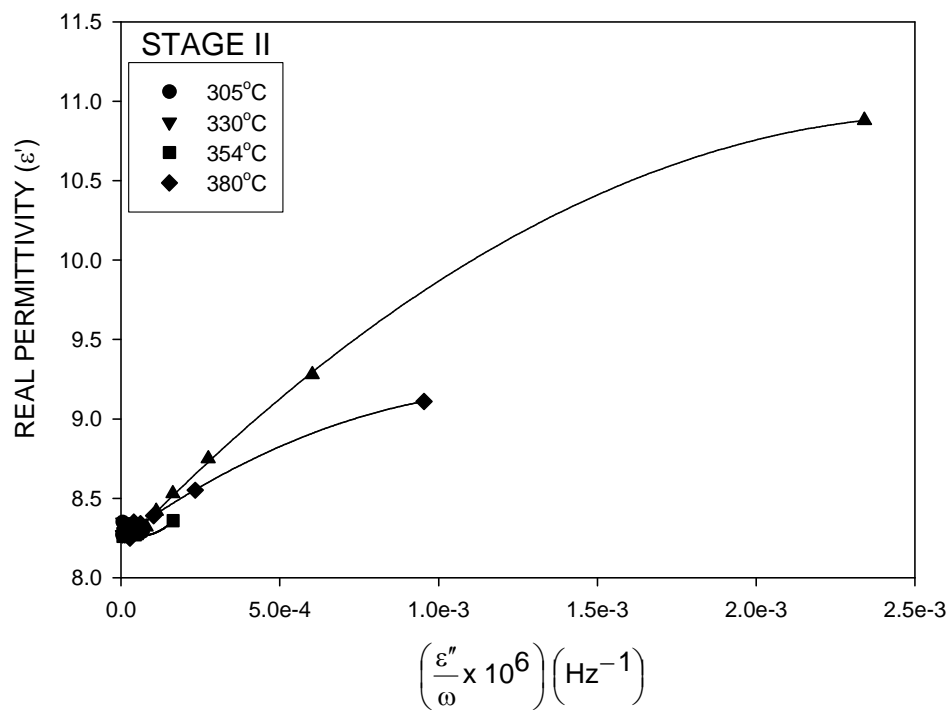


FIGURE 14 (a): Plot of  $\epsilon'$  versus  $(\epsilon''/\omega)$  for temperatures during the reaction. The heating rate was 3.2°C/min.

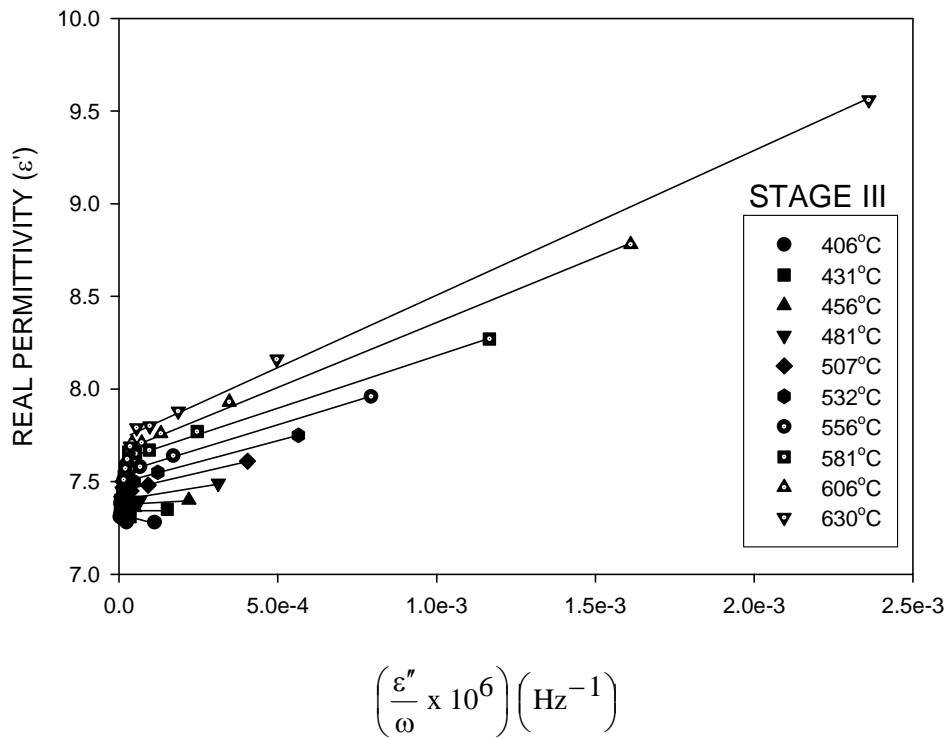


FIGURE 14 (b): Plot of  $\epsilon'$  versus  $(\epsilon''/\omega)$  for temperatures after the reaction. The heating rate was  $3.2^\circ\text{C}/\text{min}$ .

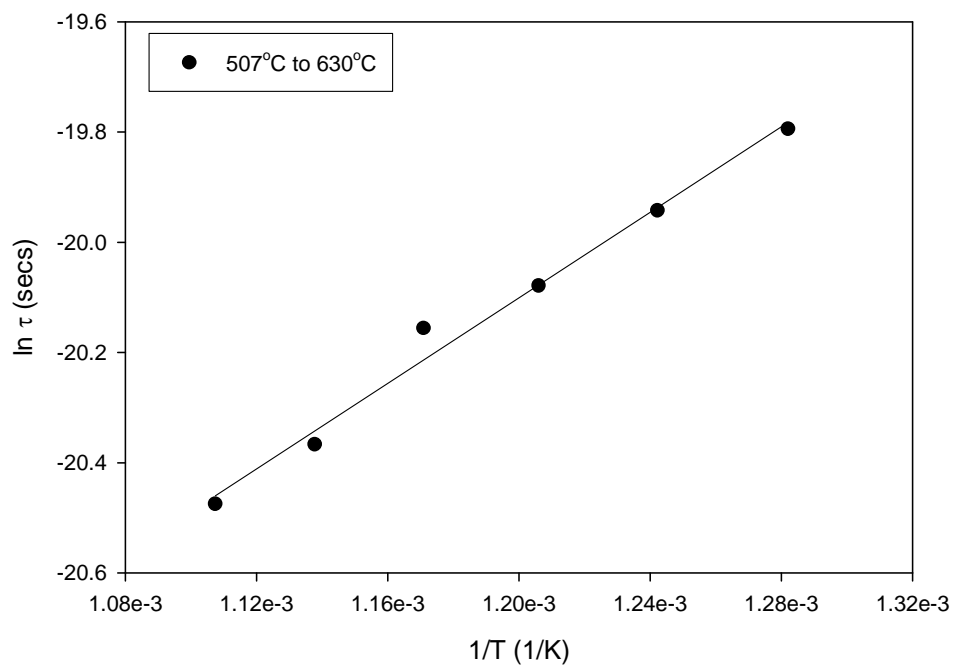


FIGURE 15: Arrhenius plot of ( $\ln \tau$ ) versus  $1/T$  for temperatures after the reaction. The heating rate was  $3.2^\circ\text{C}/\text{min}$ .